Available online at www.sciencedirect.com

jmr&t Journal of Materials Research and Technology

www.jmrt.com.br

Original Article

Tailoring thermomechanical treatment of Ni-Fe-Ga melt-spun ribbons for elastocaloric applications

E. Villa[a,*], C.O. Aguilar-Ortiz[b], A. Nespoli[a], P. Álvarez-Alonso[c], J.P. Camarillo-Garcia[b], D. Salazar[d], F. Passaretti[a], H. Flores-Zúñiga[b], H. Hosoda[e], V.A. Chernenko[d,e,f]

[a] CNR ICMATE Sede di Lecco, 23900 Lecco, Italy
[b] División de Materiales Avanzados, IPICYT, 78216 San Luis Potosí, Mexico
[c] Departamento de Física, Universidad de Oviedo, 33007 Oviedo, Spain
[d] BCMaterials & University of Basque Country (UPV/EHU), 48080 Bilbao, Spain
[e] Institute of Innovative Research (IIR), Tokyo Institute of Technology, 226-8503 Yokohama, Japan
[f] Ikerbasque, Basque Foundation for Science, 48013 Bilbao, Spain

ARTICLE INFO

Article history:
Received 3 December 2018
Accepted 31 July 2019
Available online 29 August 2019

Keywords:
Melt spun ribbons
NiFeGa
Mechanical properties
Elastocaloric effect

ABSTRACT

In the present work, the structural, mechanical and shape memory properties of $Ni_{55}Fe_{16}Ga_{29}$ (at.%) melt-spun ribbons have been studied with a prospective of application in the elastocaloric devises. Particularly, a special thermo-mechanical treatment, consisting in the thermal aging under constant external stress, was elaborated to control the residual internal stress generated due to the melt-spinning processing and improve thermomechanical and superelastic responses of the ribbon. The stress-induced entropy change was evaluated for the ribbon with improved thermomechanical properties.

1. Introduction

Shape memory alloys (SMAs) are well-known smart materials already used in medicine and industry thanking to their outstanding multifunctional properties associated with the martensitic transformation (MT), which is the physical transition used in shape memory effect and superelasticity. Recent studies in the area of novel solid state refrigeration devices incorporating the elastocaloric effect (eCE) have attracted an increasing interest in SMAs [1]. The elastocaloric effect is about the isothermal entropy change or adiabatic temperature change within a material in response to the application/removal of a stress. The particular mechanical behavior of shape memory alloys, exhibiting a superelastic flag-like-shaped stress–strain dependence due to a stress-induced MT, provides the unique condition to obtain a significant change in entropy and in temperature under their stressing. Accordingly, both the traditional SMAs (NiTi, NiTiV, NiTiCuCo, NiTiFe and CuZnAl [2–7]) and magnetic shape memory alloys (MSMAs), such as NiMnIn, NiMnInCo, NiMnInGa, NiMnGaFe, NiMnSbCo, and NiFeGa [8–13], have shown promising eCE properties. Most published works on eCE in MSMAs are concerned with com-

* Corresponding author.
E-mail: elena.villa@cnr.it (E. Villa).
https://doi.org/10.1016/j.jmrt.2019.07.067

pression tests. For instance, Camarillo et al. have found that NiMnInGa alloy exhibits the entropy change of 31 J/kgK under the applied stress change of 100 MPa, together with an adiabatic temperature change of 4.9 K [14]. Hernandez-Navarro et al. have studied eCE in NiMnInCr and obtained a reversible adiabatic temperature change of −3.9 K during unloading from 100 MPa preliminary applied along the [001] crystallographic direction of a polycrystalline textured sample [15]. Xu et al. have observed a reversible adiabatic temperature change of 4 K during a fast loading/unloading cycle of 170 MPa at room temperature for the dual-phase NiFeGa alloys [16]. On the other hand, it is worth noting that one of the first mechanical cooler prototypes is based on eCE driven by a tension [17]. From the technological and engineering points of view the tensile actuation of the small cross-sectional-shaped coolants, such as thin ribbons, films or wires, is more preferable for a cooling device than the compressive-based counterparts, where high pressure device and short-length-shaped cooling materials are needed. Therefore, taking into account the cooling applications, the ribbon-shaped MSMAs are much more attractive as the testing materials.

During time being the preparation of the ordinary SMAs as a wire, single crystal or thin film became common and technologically well elaborated, which promoted the studies of their performance in a broad range of technical applications (including mini or micro devices) [18,19]. On the other hand, the fabrication process of the bulk polycrystalline or single crystalline MSMAs is still in its infancy and generally results in materials with reduced mechanical properties due to enhanced brittleness [20]. Rapid solidification by melt-spinning can improve mechanical properties of these alloys, resulting in ribbons with the enhanced stretching performance [21–23]. Besides, this technique allows production of samples with the size and thickness adequate for the tensile or bending configurations when used, e.g., in the elastocaloric devices. Despite general advantages of the melt-spinning processing, the melt-spun ribbons face one important challenge: the resulting microstructure could be non-uniform and could contain many structural defects, which cause the internal stress. This factor, affecting directly the mechanical behavior, should be taken into account when tailoring functional characteristics of the ribbons.

Previously we have observed both anomalous shape memory and superelastic effects produced by the internal stress in the as-spun ribbons of MSMAs, NiFeGa and NiMnSn [24,25]. Particularly, in the strain versus temperature curves, $\varepsilon(T)$, under constant tensile load, a contraction of the ribbon (instead of the elongation) during the forward MT (in the cooling run) and its elongation (instead of contraction) across the reverse MT (heating path) occur. The curves restored their usual elongation/contraction appearance when the value of the applied constant stress exceeds 10 MPa [25]. The internal uniaxial compressive stress, producing the mentioned anomalous behavior, is at the origin of an inverse elastocaloric effect in MSMA ribbons [25,26]. Besides, in the aforementioned ribbons we have observed a plastic-like deformation in the stress–strain curves, $\sigma(\varepsilon)$, in martensitic state due to the rearrangement of the twin variants and partial superelastic recovery in the austenite due to the reversible stress-induced MT, which was actually small due to the enlarged brittleness of as spun ribbons [24,25].

Table 1 – Samples prepared by different thermal (TT) and thermomechanical treatments of the as-spun ribbon.

Sample	Treatment
A	As-spun
B	TT 523 K 10 min, no load
C	TT 523 K 10 min under tensile load of 50 MPa
D	TT 523 K 10 min under tensile load of 80 MPa

In this work, in order to facilitate the recrystallization process, redistribution of defects and reduction of the internal stress, whereby improve the microstructure and functional properties of ribbons in tension configuration, we have elaborated a technological procedure consisting in the thermal annealing under the applied external force. An annealing temperature for the thermal treatment was selected between 500 K, for which the beginning of the lattice defects rearrangements occurs, and 773 K, resulting in a suppression of MT due to possible $\gamma-$phase precipitation [24]. We have studied the stress-induced transformation of the thermally and thermomechanically treated ribbons by the measurements of strain versus temperature under constant load and stress versus strain at different temperatures. We have also examined the evolution of structure and microstructure of the ribbons by X-rays diffraction and optical and electron microscopies.

2. Experimental

$Ni_{55}Fe_{16}Ga_{29}$ (at.%) melt-spun ribbons with the starting martensite (M_s) and finishing austenite (A_f) temperatures equal to 359 and 371 K, respectively, were reproduced following the procedure described in [19]. The ribbon dimension was about 1 mm wide and 35 μm thick. The samples were thermally treated at 523 K for 10 min without loading and under tensile loads of 50 and 80 MPa, followed by controlled cooling at 4 K/min. As a result, four different samples were obtained as shown in Table 1.

X-ray diffraction (XRD) patterns of the ribbons faces, which were in a contact with the roller, have been recorded at room temperature and at 423 K by the X-ray diffractometer Panalytical XPert PRO with theta-2theta alignment.

Thermomechanical analysis was carried out by a Dynamic Mechanical Analyzer (DMA) Q800 from TA Instruments equipped with a liquid nitrogen cooling system. The dynamic measurements were performed at fixed frequency of 1 Hz and strain amplitude, $\varepsilon = 0.05\%$, with cooling/heating rate of 2 K/min.

The same DMA machine was used for quasi-static measurements. The strain versus temperature dependences were recorded at different applied stress values ranging from 1 to 50 MPa, with a temperature rate of 5 K/min. The stress–strain dependences were studied at different temperatures from 283 to 413 K, with a stress rate of 2.5 MPa/min. The maximum stress for each specimen was established according to the failure conditions determined for the samples tested in preliminary rounds. After each measurement, the samples were

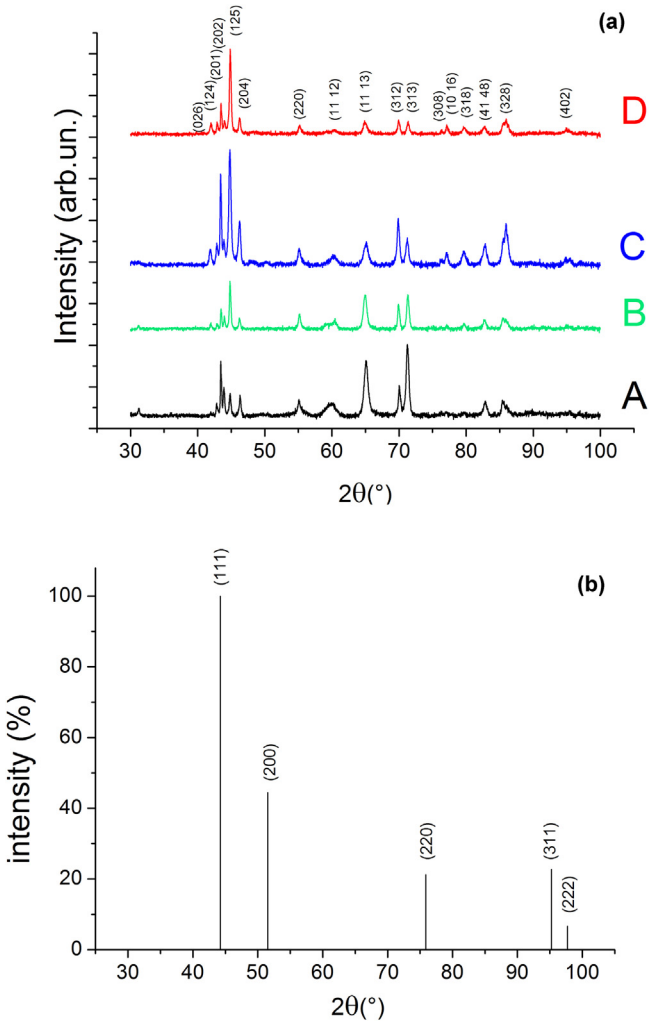

Fig. 1 – (a) Room temperature X-ray diffraction patterns for the samples (A–D) evidencing their martensitic structure. (b) Simulated XRD pattern for γ-phase as a reference.

heated (at zero load) above A_f, up to 473 K, and held for 10 min before cooling to a test temperature.

3. Results and discussion

3.1. *Structural analysis*

XRD patterns for the as-spun and thermomechanically treated ribbons (see Table 1), shown in Fig. 1(a), confirm their martensitic structure, which is well described in terms of a 10 M monoclinic lattice with P2/m space group. No extra peaks belonging to the second phase, such as γ-phase, have been observed, as it is obvious from a comparison of patterns in Fig. 1(a) with the pattern in Fig. 1(b). The important result to be highlighted is a systematic change of mutual intensities of the peaks in Fig. 1(a) depending on the ribbon treatment.

In order to analyze the evolution of the out-of-plane texture in the ribbons, the X-ray diffraction measurements were performed well above Af at 423 K, in austenite. Fig. 2 shows series of XRD patterns which are conventionally indexed in terms

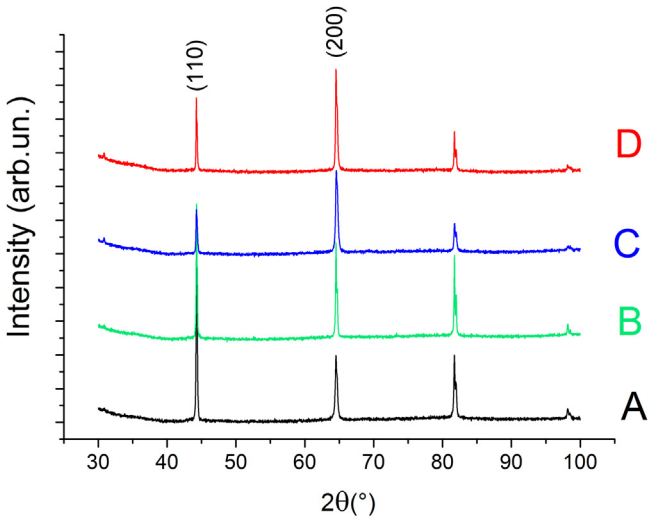

Fig. 2 – X-ray diffraction patterns measured at 423 K in the austenite phase of the samples (A–D).

of A2 cubic structure for all samples with the lattice parameter $a = 2.88$ Å (Im-3 m space group). The diffraction patterns in Fig. 2 show a strong change of the 110/200 peak intensities ratio, up to its inversion for the samples heat-treated under stress. This result becomes relevant since the mutual orientation between the crystallographic direction and the direction of the applied stress plays an important role in the elastocaloric response [25,26]. The annealing under tensile load accelerates a diffusion-activated rearrangement of the crystallographic defects that causes a change in grain structure leading to a preferential orientation of {200} atomic planes parallel to the ribbon plane. Such an orientation gives rise to the assumption about tensile stress-induced preferable orientation of <100> of recrystallized grains along the ribbon length.

3.2. *Dynamic mechanical study*

The temperature behavior of the low frequency elastic modulus, $E(T)$, was studied by the dynamic mechanical analysis. The results, shown in Fig.3 present a hysteretic behavior, typical for the first order MT. A cooling in austenite results in some decreasing of the elastic modulus due to the lattice softening on approaching MT. During further cooling, the forward MT into martensitic phase proceeds accompanied by the modulus, E, sharp increase. A significant difference in $E(T)$ values among the samples can be attributed to the strengthening of the ribbon after annealing under stress. The strengthening may be produced by the changes in the grain structure. One cannot also exclude an influence of a little amount of γ-precipitates which hardly can be detected by XRD but may be formed as a result of such a treatment, as, e.g., it was observed for Ni-Mn-Ga bulk alloys [27]. Due to instrumental limitations of the DMA machine, such as: (i) thermocouple is situated very close to the sample but not attached to it; and (ii) cooling ramps are better temperature controlled than heating ones, the transformation temperatures obtained during cooling are more reliable and their absolute values can be accepted within ± 5 K of uncertainty. The transition temperatures were

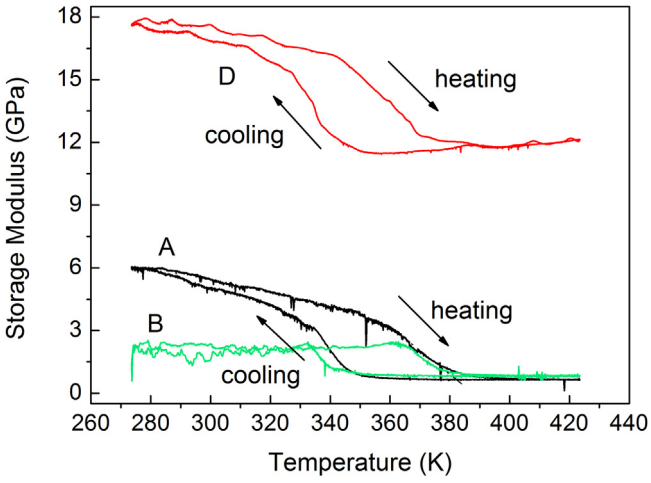

Fig. 3 – Temperature dependencies of the elastic modulus for samples (A–D).

obtained by a standard two-tangent method, whereby the as-spun ribbon, sample A, has $M_s = 348$ K. This value is in a good agreement with the value reported in [22] for the same composition ribbon prepared in different series. Other samples show slightly smaller values of M_s which are within the indicated uncertainty. This means that thermomechanical treatment has a minimal influence on the transformation temperature of MT.

3.3. *Temperature dependences of transformation strains exhibited by ribbons under tensile load*

Temperature dependences of the MT-induced spontaneous deformation of the ribbons loaded by a constant tensile stress in the DMA machine are presented in Fig. 4. The curves in Fig. 4(a), obtained under small tensile stress, 5 MPa, show drastic changes of the transformation-induced strain evolution depending on their treatment. The ribbons A and B during cooling demonstrate at the forward MT a progressively reduced contraction, instead of the expected elongation, whereas no contraction, only an elongation was observed for the ribbons C and D.

Such an unusual "inverse" behavior of the transformation strain in the ribbons A and B was observed in the as-spun Ni-Mn-Sn and Ni-Fe-Ga SMA ribbons and bulk Ni-Ti SMA preliminary aged under constraint conditions [28,29]. The interesting point is that a relatively short heat treatment itself reduces but not eliminates the "inverse" effect. Fig. 4(a) demonstrates that the "inverse" effect disappears only if the same heat treatment is performed under applied stress. According to [28], the mentioned "inverse" effect is produced by the compressive internal stresses existing in the as-spun ribbons giving rise to the phenomenon of the inverse elastocaloric effect (eCE). The curves for samples C and D show that the thermal treatment under a tensile load tends to cancel a virgin internal compressive stress. According to the data in Fig. 4, the internal stress in the ribbon is already eliminated after the treatment at 50 MPa and higher stress is more than enough for this purpose. On the other hand, the stress–strain behavior described in the next section shows that the treatment at 80 MPa provides some evidence of the larger martensitic plasticity of the ribbon if compared to the treatment at 50 MPa. More studies are needed to determine the optimal value of the stress in this case.

It is implied that the thermo-mechanical treatment in the case of C and D ribbons promotes the microstructural changes more effectively than a simple annealing, facilitating the same sign of a strain and the applied stress along the ribbon longitudinal direction, whereby switching the ribbon from the inverse to the conventional regime of eCE already at the low stress values. This switching is indirectly illustrated by considering the sign inversion of the isothermal stress-induced entropy change, ΔS, which is expressed by the Maxwell relationship as [30]:

$$\Delta S(T,\sigma) = \int_0^{\sigma} \frac{\partial \varepsilon(T,\sigma)}{\partial T} d\sigma \quad (1)$$

The inset to Fig. 4(a) presents the $\frac{\partial \varepsilon(T,\sigma)}{\partial T}$ versus T curves for the samples A and D. Referring to the sign of $\frac{\partial \varepsilon(T,\sigma)}{\partial T}$ in the expression for ΔS, the sample A exhibits under the external stress of 5 MPa a positive change in entropy (inverse eCE) associated with the inverse mechanical behavior due to a larger internal stress (more than 5 MPa) acting against the tensile applied stress. The thermal treatment under stress removes completely this effect and, at the same stress value, the temperature dependence of $\frac{\partial \varepsilon(T,\sigma)}{\partial T}$ reflects a conventional entropy change usually observed in the stress-induced MT in the elastocaloric applications.

Fig. 4(b) shows the temperature dependences of strain under the applied stress of 40 MPa for all the samples. At this level of stress, the $\varepsilon(T)$ curves present a conventional sharp elongation/contraction of ribbons across the forward/reverse MT, which is manifestation of the pronounced shape memory effect. Note that the strain recovery is accompanied by a generation of the reversion stress, which means that the ribbons can produce mechanical work. The sample D (and partially C) exhibits a larger recovery strain, of about 1.2% compared to 0.7% and 1.0% for samples A and B, respectively, which implies its enhanced martensitic plasticity. To this end, much more convincing are the results of $\varepsilon(T)$ experiments performed under higher stresses. The as-cast or thermally treated ribbons A and B fail at MT if loaded by more than 50 MPa, whereas ribbons C and D can be cycled through MT under different loads, up to 150 MPa, showing unsurpassed thermomechanical performance. Fig. 4(c) illustrates the high enough mechanical strength and enhanced ductility of the ribbon C. This specimen shows recovery strain of about 1.5% under 150 MPa and at this highest stress a residual plastic deformation of 0.5% occurs. Curves, shown in Fig. 4(c), were used to determine the values of the martensitic starting temperatures as a function of stress. As a result, the linear dependence with a slope of 4.3 MPa/K is obtained as shown in Fig. 4(d).

Eq. (1) and $\varepsilon(T,\sigma)$ data in Fig. 4(c) were used to calculate the stress induced entropy change, ΔS, corresponding to the forward austenite-martensite transformation in the sample C. The obtained $\Delta S(T)$ results at different constant

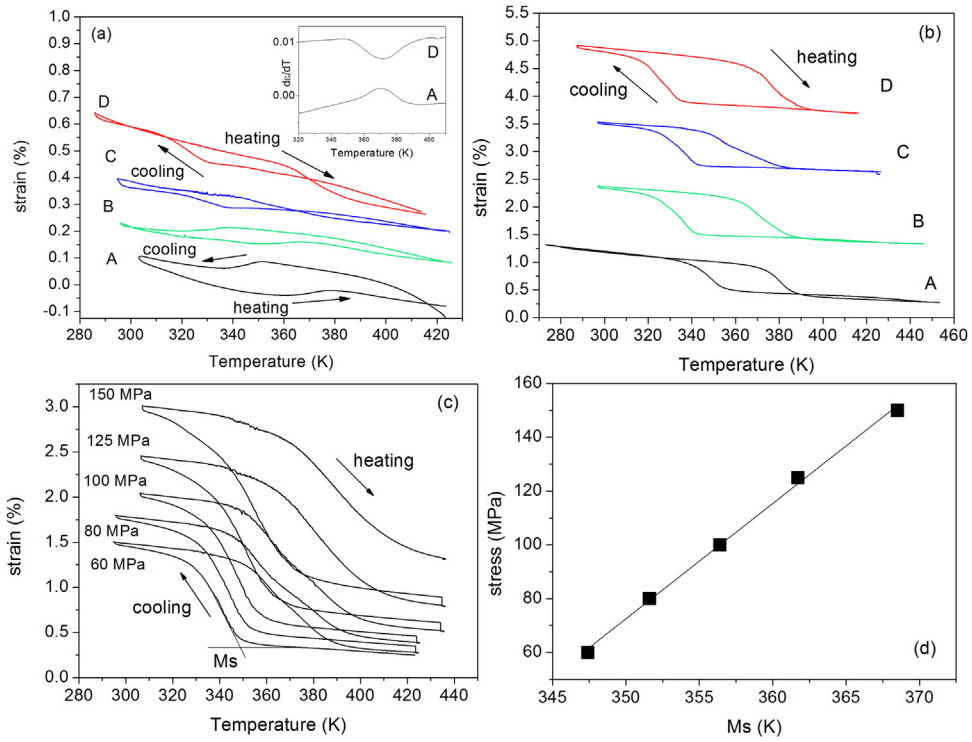

Fig. 4 – Temperature dependences of strain exhibited by all ribbons loaded with stress of 5 MPa (a) and 40 MPa (b). Inset to Fig. 4(a) depicts $\frac{\partial\varepsilon(T,\sigma)}{\partial T}$ versus T curves for ribbons A and D on heating. The curves are shifted along Y-axis to avoid overlapping. (c) Behavior of the transformation strain for ribbon C loaded under different constant stresses up to 150 MPa; (d) stress dependence of the MT temperature, Ms, for sample C. Line is the linear fit.

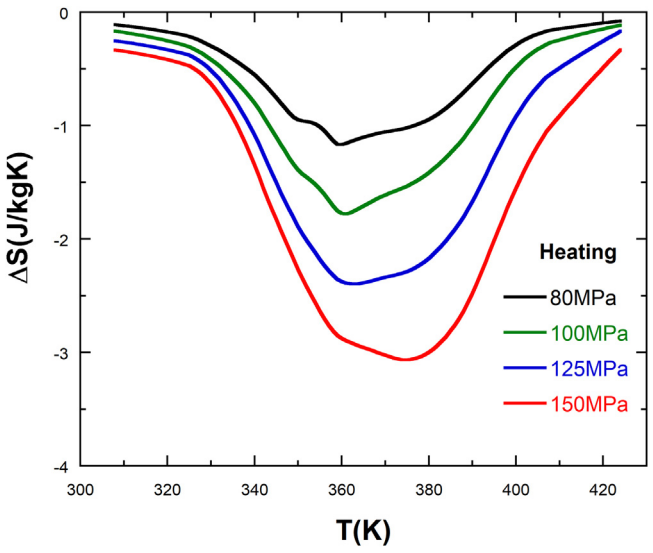

Fig. 5 – Temperature dependence of the stress induced entropy change for specimen C.

stresses are shown in Fig. 5. As expected from the temperature dependences of the elongation across the martensitic transformation (see Fig. 4(c)), the entropy change exhibits a negative peak (i.e., showing a conventional elastocaloric effect) for each applied stress. Following Khan et al. [31], it is instructive to emphasize that a combination of the several caloric effects, such as eCE and magnetocaloric effect (MCE), can essentially enhance the refrigerant capability if their entropy change peaks possess the same sign. Although data for magnetocaloric effect in NiFeGa ribbons are not available in the literature, the MCE response for bulk specimens should be conventionally with the same sign of peak of the magnetic field induced entropy change as the eCE peak at the forward martensite transformation [32]. Such a possibility makes this composition interesting for further research on the multicaloric effects. Furthermore, Fig. 5 shows that the absolute value of the entropy change increases with stress (up to −3.1 J/kgK under an applied stress of 150 MPa), since the specimen shrinks during the reverse martensitic transition on heating. This contrasts, to some extent, with the behavior observed in the as-cast NiFeGa ribbons, in which the existence of a compressive internal stress leads to a gradual change from the inverse elastocaloric effect for small stresses to a conventional eCE for stresses above 20 MPa [28].

3.4. *Stress–strain dependences at different temperatures*

Fig. 6 reports the stress–strain curves obtained in the martensitic state at 343 K (close to M_s). The linear parts of curves can be attributed to the elastic deformation. The nonlinear parts of curves and residual strains after unloading of the samples are produced by a rearrangement of the twin structure, which is confirmed by the temperature induced strain recovery during heating of the samples across the reverse MT up to 473 K.

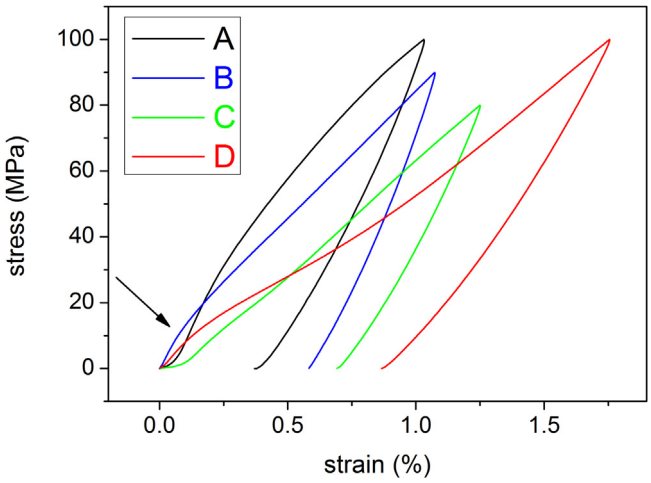

Fig. 6 – Stress–strain curves for all ribbons measured in the martensitic state, at 343 K. The arrow indicates the stress value corresponding the start of detwinning.

The shapes of curves indicate that the samples C and D have a much smaller detwinning stress than A and B. As a result, the former ribbons accumulate a much larger recoverable strain under similar values of the stress. Generally, the melt-spun ribbons preserve an internal stress and solidification defects which strongly affect the detwinning process in martensite or the stress-induced martensitic transformation, whereby no iso-stress plateau is observed [33], as also demonstrated in the present work. Only in some SMAs ribbons, like NiTi or NiTiCu [34], it is possible to obtain the quite developed flag-shaped stress–strain loops.

Likewise for the results of $\varepsilon(T)$ tests, the stress–strain behavior of the ribbons A and B has also a brittle character, especially in the austenitic cubic phase. It is found that the loading of these ribbons caused an almost linear increase of the strain, which terminated at 80–100 MPa due to the sample failure. No clear indication about the formation of stress-induced martensitic phase was observed. On the other hand, the samples C and D, thermally treated under load, demonstrate a high enough strength and a well-pronounced superelastic behavior, reflected in the flag-like shaped stress–strain curves, with more than 2% of reversible strain and small residual strains as illustrated in Fig. 7(a). This figure presents an evolution of the stress–strain curves for sample D measured in a cubic phase at different temperatures. The values of the martensitic start critical stresses were extracted from the superelastic curves shown in Fig. 7(a) and plotted as a function temperature in Fig. 7(b). The dependence obtained can be approximated by a straight line with a slope of 3.2 MPa/K, which is in a rough agreement with the coefficient obtained in the strain – temperature tests for sample C (Fig.4(d)). This value of slope is essentially larger than the previously obtained one for the as-spun ribbon A, which was actually studied up to 40 MPa only [28], and can be compared with the value of about 2 MPa/K, evaluated from the tensile data for single crystalline $Ni_{54}Ga_{27}Fe_{19}$ exhibiting cubic-orthorhombic MT [35].

4. Summary and conclusions

Tailoring the thermomechanical behavior of melt-spun ribbons is one of the challenging tasks in their elastocaloric applications. In this work we have found that the thermomechanical properties of Ni-Fe-Ga shape memory ribbons, promising for elastocaloric applications, can be improved by the treatment of these materials consisting in the annealing under tensile stress. It was shown that annealing under stress accelerates a recrystallization of the ribbon manifested in both the changes of crystallographic texture and the disappearance of internal stress, which can be attributed to the rearrangement of defects, such as the vacancies, dislocations, grain boundaries etc. The separated studies are needed to clarify the nature and role of the defects affected by the thermomechanical treatment. The thermomechanically treated ribbons exhibit a conventional elastocaloric effect at all values of stresses, whereas the as-quenched and annealed ribbons present an inverse elastocaloric effect under low applied stresses. By structural and thermomechanical measurements, evidences have been found that the thermal treatment under applied tensile load along longitudinal direction of ribbon is an efficient route to remove the internal stress produced during the rapid solidification process and to modify a microstructure, whereby improving shape memory and superelastic properties of the ribbons. Besides, Ni-Fe-Ga

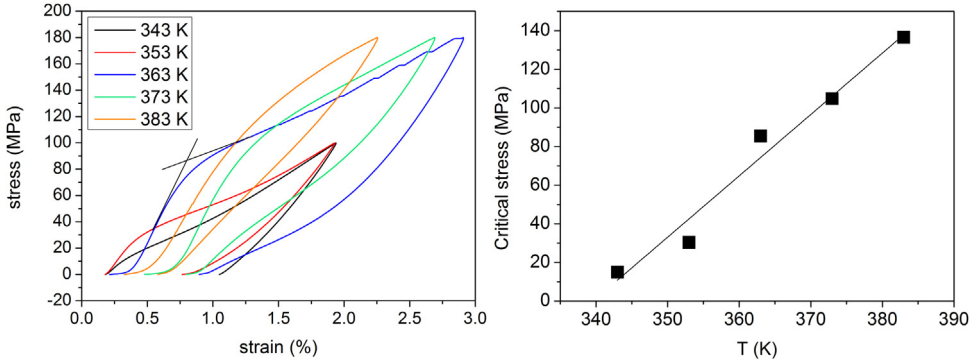

Fig. 7 – (a) Stress–strain dependences of the austenite at different temperatures for sample D; (b) critical stress values versus temperature extracted from curves shown in Fig.7(a). The two-tangent method of determination of critical stress is shown on one of the curves in Fig. 7(a).

MSMAs are promising for the application in cooling devices exploiting the combination of the magnetocaloric and elastocaloric responses.

Acknowledgements

This work has been carried out with the financial support of the Spanish Ministry of Economy and Competitiveness (Project no. RTI2018-094683-B-C53), Asturias Government (FC-15-GRUPIN14-037 245), and Basque Government Department of Education (project IT711-13).

REFERENCES

[1] Crossley S, Mathur ND, Moya X. AIP Adv 2015;5:67153.
[2] Cui J, Wu Y, Muehlbauer J, Hwang Y, Radermacher R, Fackler S, et al. Appl Phys Lett 2012;101:73904.
[3] Mañosa L, Jarque-Farnos S, Vives E, Planes A. Appl Phys Lett 2013;103:211904.
[4] Ossmer H, Lambrecht F, Gultig M, Chluba C, Quandt E, Kohl M. Acta Mat 2014;81:9–20.
[5] Ossmer H, Miyazaki S, Kohl M. Mater Today: Proc 2015;2(3):971–4.
[6] Ossmer H, Chluba C, Kauffmann-Weiss S. APL Mater 2016;4.6:064102.
[7] Min-Gu Jo YK, Park J-W, Park H-K, Han HN. Scr Mater 2018;144:48–51.
[8] Lu B, Xiao F, Yan A, Liu J. Appl Phys Lett 2014;105:161905.
[9] Soto-Parra DE, Vives E, González-Alonso D, Mañosa L, Planes A, Romero R, et al. Appl Phys Lett 2010;96:71912.
[10] Millán-Solsona R, Stern-Taulats E, Vives E, Planes A, Sharma J, Nayak AK, et al. Appl Phys Lett 2014;105:241901.
[11] Pataky GJ, Ertekin E, Sehitoglu H. Acta Mater 2015;96:420–7.
[12] Camarillo JP, Aguilar-Ortiz CO, Flores-Zúñiga H, Ríos-Jara D, Soto-Parra DE, Stern-Taulats E, et al. Funct Mater Lett 2017;10:1740007.
[13] Yang Z, Cong DY, Sun XM, Nie ZH, Wang YD. Acta Mater 2017;127:33–42.
[14] Camarillo J-P, Aguilar-Ortiz C-O, Flores-Zúñiga H, Ríos-Jara D, Soto-Parra D-E, Stern-Taulats E, et al. Funct Mater Lett 2017;10:1740007, http://dx.doi.org/10.1142/S1793604717400070.
[15] Henández-Navarro F, Camarillo-Garcia J-P, Aguilar-Ortiz C-O, Flores-Zúñiga H, Ríos D, González J-G, et al. Appl Phys Lett 2018;112:164101, http://dx.doi.org/10.1063/1.5018732.
[16] Xu Y, Lu B, Sun W, Yan A, Liu J. Appl Phys Lett 2015;106:201903, http://dx.doi.org/10.1063/1.4921531.
[17] Qian S, Geng Y, Wang Y, Ling J, Hwang Y, Radermacher R, et al. Int J Refrig 2016;64:1–19, http://dx.doi.org/10.1016/j.ijrefrig.2015.12.001.
[18] Nespoli A, Biffi CA, Previtali B, Villa E, Tuissi A. Metall Mater Trans 2014;A45:2242–9.
[19] Nespoli A, Bassani E, Besseghini S, Villa E. EMRS 2010 Proceedings. Phys Procedia 2010;10:182–8.
[20] Besseghini S, Villa E, Passaretti F, Pini M, Bonfanti F. Mater Sci Eng A 2004;378:415–8.
[21] Panda AK, Kumar A, Ghosh M, Mitra A. J Magn Magn Mater 2008;320(20):e730–3.
[22] Albertini F, Besseghini S, Paoluzi A, Pareti L, Pasquale M, Passaretti F, et al. J Magn Magn Mater 2002;242-245:1421–4.
[23] Wu Y, Wang J, He Y, Wu H, Jiang C, Xu Hn. Acta Mater 2016;104:91–100.
[24] Villa E, Agilar-Ortiz CO, Álvarez-Alonso P, Camarillo JP, Lara-Rodriguez GA, Flores-Zúñiga H, et al. MATEC web of conferences, 33. 2015. p. 05009.
[25] Bruno NM, Karaman I, Chumlyakov YI. Phys Status Solidi B 2018;255:1700437.
[26] Hernández-Navarro F, Camarillo-Garcia JP, Aguilar-Ortiz CO, Flores-Zúñiga H, Ríos D, González JG, et al. App Phys Lett 2018;112:164101.
[27] Pérez-Checa A, Feuchtwanger J, Barandiaran JM, Chernenko VA. J Alloys Compd 2018;741:148–54, http://dx.doi.org/10.1016/j.jallcom.2018.01.068.
[28] Álvarez-Alonso P, Aguilar-Ortiz CO, Villa E, Nespoli A, Flores-Zúñiga H, Chernenko VA. Scr Mater 2017;128:36–40.
[29] Xiao F, Fukuda T, Kakeshita T. Scr Mater 2016;124:133–7.
[30] Mañosa L, Planes A, Acet M. J Mater Chem A 2013;1:4925.
[31] Khan MT, Wang Y, Wang C, Liao X, Yang S, Song X, et al. Scr Mater 2018;146:182–6, http://dx.doi.org/10.1016/j.scriptamat.2017.11.041.
[32] Yu HJ, Fu H, Zeng ZM, Sun JX, Wang ZG, Zhou WL, et al. J Alloys Compd 2009;477:732–5, http://dx.doi.org/10.1016/j.jallcom.2008.10.143.
[33] Chernenko VA, Kanth BR, Mukhopadhyay PK, Kaul SN, Villa E, Gambardella A, et al. Appl Phys Lett 2008;93:141904.
[34] Kim M, Noh J, Cho G, Kim Y, Liu Y, Nam T, et al. J Alloys Compd 2013;577S:S179–83.
[35] Sutou Y, Kamiya N, Omori T, Kainuma R, Ishida K, Oikawa K. Appl Phys Lett 2004;84:1275.